^{177}Lu-Labeled Eu-Doped Mesoporous SiO$_2$ Nanoparticles as a Theranostic Radiopharmaceutical for Colorectal Cancer

Rodrigo da Silva Viana, Luciana Amaral de Mescana Costa, Ashlyn C. Harmon, Manoel Adrião Gomes Filho, Eduardo H. L. Falcão, Maria G. H. Vicente, Severino A. Junior,* and J. Michael Mathis*

Read Online

ACCESS | Metrics & More | Article Recommendations | Supporting Information

ABSTRACT: Colorectal cancer is one of the most significant types of cancer, ranking second in the world's mortality cases. As colorectal cancer is often diagnosed at a late stage of disease progression, effective treatments are necessary. Therefore, radiotherapy has become a fundamental approach in the treatment of colorectal cancer, especially those based on the use of ^{177}Lu. A potential approach to meet this challenge is the use of nanotechnology through the development of radionuclide-based nanomaterials. In this work, we investigated a SiO$_2$-derived class of nanomaterials formed by the insertion of the coordination complex, based on Eu^{3+} and pyrimidine-2,6-dicarboxylic acid (DPA), into nanoparticles of amino-functionalized mesoporous silica (EuDPA/SiO$_2$−NH$_2$). The properties of the EuDPA/SiO$_2$−NH$_2$ nanoparticles were initially investigated by SEM, FT-IR, TGA, and luminescence. The cellular uptake of EuDPA/SiO$_2$−NH$_2$ nanoparticles into HT-29 cells was confirmed by fluorescence microscopy. Radioactivity was incorporated into the EuDPA/SiO$_2$−NH$_2$ nanoparticles by replacing a tracer quantity of Eu^{3+} sites with the lanthanide element ^{177}Lu, which resulted in the composition of a dual-modality probe for both SPECT imaging and tumor radiotherapy. Analysis of ^{177}Lu loading into EuDPA/SiO$_2$−NH$_2$ particles showed efficient incorporation, up to 93% radioactivity into the final compound. The imaging potential of the ^{177}Lu−EuDPA/SiO$_2$−NH$_2$ nanoparticles was investigated by SPECT/CT imaging, a subcutaneous HT-29 mouse model of colorectal cancer. Image analysis showed that tumor localization was maintained after intratumoral administration for up to 48 h. To evaluate the therapeutic potential of ^{177}Lu−EuDPA/SiO$_2$−NH$_2$ nanoparticles, HT-29 xenografts were treated *in vivo* by direct intratumoral injection. Compared with control (PBS) treatment or treatment with unlabeled EuDPA/SiO$_2$−NH$_2$ nanoparticles, the treatment with ^{177}Lu−EuDPA/SiO$_2$−NH$_2$ nanoparticles resulted in a significantly reduced tumor growth. Together, the results of this study results indicate that ^{177}Lu−EuDPA/SiO$_2$−NH$_2$ is a promising agent for further development in SPECT imaging and clinical treatment of colorectal cancer.

KEYWORDS: colorectal cancer, coordination compound, dipicolinic acid, HT-29, lutetium-177, nanoparticle photoluminescence, radiotherapy, SPECT imaging

1. INTRODUCTION

Colorectal cancer is one of the most significant health issues worldwide; it is estimated that colorectal cancer is the third most common cancer, with an estimated 1.8 million new cases diagnosed each year.[1] Because colorectal cancer is often diagnosed at a late stage of disease progression, about 900000 individuals die annually globally, making this malignancy the second leading cause of cancer death.[1] Thus, the development of effective treatments is sorely needed.

In addition to surgery and chemotherapy, radiotherapy has become a mainstay approach for treating colon cancer. There are two different approaches to radiotherapy:[2] (1) using electromagnetic radiation (i.e., ionizing radiation typically used for external beam radiotherapy) or (2) particle radiation (i.e., radioisotopes emitting α, β^-, or Auger electron particles). The

β-emitting radioisotopes, including ^{131}I, ^{90}Y, ^{177}Lu, and ^{186}Re, have received considerable attention in recent years for particle radiation therapy because they are readily available, have favorable emission characteristics, and are accessible to straightforward radiochemistry technologies.
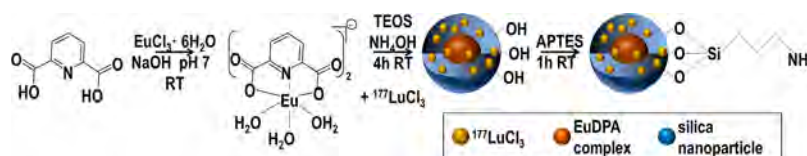
In particular, ^{177}Lu (half-life 6.7 days) has emerged as an ideal dual-modality radionuclide. In essence, it is a medium-

Figure 1. Schematic depiction of the ^{177}Lu−EuDPA/SiO$_2$−NH$_2$ hybrid nanoparticle synthesis.

energy β-emitter (at 490 keV) for radiotherapy application, and it emits low-energy γ-rays (at 208 and 113 keV), which are useful for diagnostic imaging by SPECT (single photon emission computerized tomography).[3]

Beta particles emitted from ^{177}Lu decay travel relatively short distances in tissue (1−2 mm).[4] In locoregional applications, the resulting energy can be absorbed by the disease target sites, killing the cancer cells without having damaging effects on surrounding normal tissues.[5] There is a need to improve further the therapeutic efficacy of radiotherapy using radionuclides such as ^{177}Lu by identifying alternative approaches for delivering these agents to a tumor site. One potential approach to address this challenge is to utilize nanotechnology for targeted delivery through the development of multifunctional nanomaterials.[6]

Radiolabeled nanoparticles represent a class of agents that has been recognized to have enormous potential for clinical oncology applications.[7] Recent trends in nuclear medicine are aimed at exploiting these materials in a multifunctional approach, in which these systems are engineered with combined properties of molecular detection and therapeutic capabilities, known as theranostics.[8] The success of this approach depends on the property choice of radionuclides for incorporation into a nanoparticle platform. For example, γ-emitters with energy in the 150 keV range have been useful in the context of SPECT imaging, while those radioisotopes that are also β-emitters are capable of producing therapeutic cellular damage and cell death.[7,8]

Currently, the choice of these nanomaterials in colorectal cancer therapy has grown considerably,[9] which can be represented by inorganic compounds (i.e., carbon nanotubes,[10] silica nanoparticles,[11] gold nanoparticles,[12] magnetic nanoparticles,[13] quantum dots,[14] etc.) and organic compounds (i.e., natural compounds,[15,16] polymeric micelles,[17] liposomes,[18] dendrimers,[19] etc.). As shown in Figure 1, we developed a novel class of nanomaterials, in which lanthanide coordination complexes of Eu^{3+} and pyridine-2,6-dicarboxylic acid (H$_2$DPA) were coupled into amino-functionalized mesoporous silica nanoparticles (EuDPA/SiO$_2$−NH$_2$), and ^{177}LuCl$_3$ was incorporated.

Silica nanoparticles have been exploited for numerous biomedical applications based on their biocompatibility, low toxicity, and capability of precise control over nanostructure synthesis.[20] In addition, surface modifications of silica nanoparticles are possible, allowing for modulation of drug loading, pharmacokinetics, and targeted delivery.[21] We examined the characteristics of the EuDPA/SiO$_2$−NH$_2$ nanoparticles by SEM, FT-IR, TGA, and luminescence to define their chemical, morphological, and optical properties for the application of interest. We also determined the cellular uptake of EuDPA/SiO$_2$−NH$_2$ nanoparticles into the human HT-29 colon cancer cell line.

Radioactivity was also incorporated into the EuDPA/SiO$_2$−NH$_2$ nanoparticles by adding a tracer amount of the lanthanide element ^{177}Lu into the Eu^{3+} sites of the nanostructure, resulting in the composition of a dual-modality probe capable of both SPECT imaging and tumor radiotherapy. After determining the efficiency of ^{177}Lu incorporation into the EuDPA/SiO$_2$−NH$_2$ nanoparticles, we performed SPECT/CT imaging and biodistribution studies to assess uptake *in vivo* in mice. Finally, the antitumor efficacy of ^{177}Lu−EuDPA/SiO$_2$−NH$_2$ nanoparticle radiotherapy treatment was evaluated by using an HT-29 tumor xenograft mouse model. Together, these results demonstrate the potential use of ^{177}Lu−EuDPA/SiO$_2$−NH$_2$ as a colon cancer therapeutic agent and support further *in vitro* and *in vivo* investigations.

2. MATERIALS AND METHODS

2.1. Reagents. All experimental procedures were performed by using analytical grade reagents purchased commercially from Sigma-Aldrich (St. Louis, MO).

2.2. Synthesis of the EuDPA Coordination Compound. The EuDPA complex was synthesized by using the method described by Tao et al.[22] For this approach, 0.343 g of H$_2$DPA (2 mmol) was added to 20 mL of ethanol under stirring conditions. After that, 1 M NaOH(aq) portions were added dropwise until the solution reached pH = 7. Finally, 0.366 g of EuCl$_3$·6H$_2$O (1 mmol) was dissolved in another 20 mL of ethanol. A precipitate was produced by the dropwise addition of the EuCl$_3$·6H$_2$O in ethanol. Subsequently, the precipitate was filtered, washed with ethanol, and stored in a clean, dry flask.

2.3. Synthesis of EuDPA/SiO$_2$−NH$_2$ Hybrid Nanoparticles. For the synthesis of the hybrid nanoparticles, an adaptation of the Stober sol−gel method[23,24] was used to incorporate the EuDPA complex into the matrix of silica nanoparticles. This methodology consists of mixing 30 μL/0.09 mmol of EuDPA(aq) (2 mg/mL), 20 μL of NH$_4$OH, and 27 μL of tetraethyl orthosilicate (TEOS) for 4 h under agitation at ambient temperature. Afterward, the mixture was added to 5.2 μL of 3-aminopropyltriethoxysilane (APTES), and the mixture was stirred for another 1 h. Finally, the resulting material was transferred to a 15 mL centrifuge tube and centrifuged for 10 min at 8000 rpm. The centrifugation procedure was repeated three more times by using 1 mL of ultrapure water to wash the material.

2.4. Synthesis of Lu$_{0.5}$−Eu$_{0.5}$DPA/SiO$_2$−NH$_2$ Hybrid Nanoparticles. The same protocol used for the synthesis of EuDPA/SiO$_2$−NH$_2$ was repeated, altering only the addition of 0.045 mmol of EuDPA(aq) and 0.045 mmol of LuCl$_3$·6H$_2$O(aq) in a volume of 30 μL of water instead of only 0.09 mmol of EuDPA(aq) as previously described.

2.5. Synthesis of ^{177}Lu−EuDPA/SiO$_2$−NH$_2$ Hybrid Nanoparticles. A mixture was prepared from EuDPA(aq) (2 mg/mL), 5 μL of ^{177}LuCl$_3$ (37−111 MBq; 1−3 mCi), 20 μL of NH$_4$OH, and 10 μL of TEOS, which was stirred for 4 h under stirring at ambient temperature. Afterward, 5.2 μL of APTES was added, and the mixture was stirred for an additional 1 h. Finally, the material was transferred to a 1.5 mL microcentrifuge tube and centrifuged for 10 min at 8000 rpm. The centrifugation procedure was repeated three more times by using 1 mL of water to wash the material, and the radioactivity of the supernatant and the solid material obtained after centrifugation was recorded. After the washing procedure, the ^{177}Lu−EuDPA/SiO$_2$−NH$_2$ product was obtained as a white solid.

2.6. Nanoparticle Characterization. Fourier transform infrared (FT-IR) spectroscopy was measured at 4000−650 cm^{-1} on a Bruker spectrometer (model Tensor 27) equipped with a Pike single-bounce diamond/ZnSe ATR cell. Scanning electron microscopy (SEM)

images were acquired on a low-vacuum scanning electron microscope (JEOL JSM-6610LV) coupled with an energy dispersive X-ray spectrometer (EDS). EDS analysis was obtained with an angle of 45°. Transmission electron microscopy (TEM) images were obtained on a CCD camera coupled FEI microscope (model Morgagni 268 D), with an acceleration voltage 40−100 kV, point resolution 0.45 nm, line resolution 0.34 nm, and magnification up to 180000×. The dynamic light scattering (DLS) analysis was performed on a Microtrac Zeta Trac 150 particle counter (model/series: S3000/S3500). The thermogravimetric (TGA) analyses were performed by using a Shimadzu thermal analyzer (model DTG-60/60H) in atmospheric air.

The photoluminescence properties were investigated using a Fluorolog-3 spectrofluorometer (model FL3-22TAU3; Jobin-Yvon, Edison, NJ) equipped with a continuous 450 W xenon lamp and UV xenon flash tube for excitation and a double-grating monochromator in the excitation and emission positions. The emission spectra were corrected for the wavelength-dependent response of the detection system. A silicon photodiode reference detector was used to monitor and compensate for the variation in the xenon lamp output by using typical correction spectra provided by the manufacturer. The experimental coefficients of spontaneous emission, A_{0J}, are obtained according to the relation

$$A_{0J} = A_{01}\left(\frac{I_{0J}}{I_{01}}\right)\left(\frac{\nu_{01}}{\nu_{0J}}\right) \tag{1}$$

where I_{01} and I_{0J} are the integrated intensities of the $^5D_0 \rightarrow {}^7F_1$ and $^5D_0 \rightarrow {}^7F_J$ transitions (J = 0, 2, 3, and 4) with ν_{01} and ν_{0J} energy barycenters, respectively. The coefficient of emission spontaneous, A_{01} in eq 1, is given by the expression $A_{01} = 0.31 \times 10^{-11}(n)^3(\nu_{01})^3$, and its value is estimated to be 50 s^{-1}.[25]

The emission quantum efficiency (η) was calculated according to eq 2

$$\eta = \frac{A_{rad}}{A_{rad} + A_{nrad}} \times 100 \tag{2}$$

where A_{rad} is the radiative decay rate obtained by summing over the experimental coefficients of spontaneous emission A_{0J} for each $^5D_0 \rightarrow {}^7F_J$ (J = 0−4) transition. The total radiative decay rate (A_{total}) is given by the relation $A_{total} = \tau^{-1}$, where τ is the lifetime for the radiative decay associated with the $^5D_0 \rightarrow {}^7F_2$ transition. Finally, the nonradiative decay rate (A_{nrad}) was determined by the difference $A_{nrad} = A_{total} - A_{rad}$.[26,27]

2.7. Cell Culture. The human colon adenocarcinoma cell line, HT-29, was obtained from the American Type Culture Collection (Manassas, VA) and grown in Dulbecco's modified Eagle's medium (DMEM) supplemented with 10% fetal bovine serum, 50 U/mL penicillin, and 50 mg/mL streptomycin. The cultured HT-29 cells were maintained in 5% CO$_2$ at 37 °C under a humidified atmosphere condition.

2.8. Confocal Microscopy. The HT-29 cells were plated into 35 mm glass-bottom cell culture dishes (Thermo Fisher Scientific, Waltham, MA) at a density of 1.5×10^5 per dish for confocal microscopy. After 24 h, the cells were treated with 10, 100, and 1000 μg/mL of each nanoparticle preparation for an additional 24 h. Subsequently, the medium was removed, and the cells were incubated for 10 min with 1 mL of phosphate-buffered saline (PBS) containing 5 μL of Hoechst 33342 dye. Subsequently, the cells were washed three times with 1 mL of PBS and visualized by confocal microscopy using a Leica SP8 confocal microscope platform with a white light laser source.

2.9. XTT (2,3-Bis(2-methoxy-4-nitro-5-sulfophenyl)-2H-tetrazolium-5-carboxanilide) Cytotoxicity Assay. The cell cytotoxicity after treatment with EuDPA/SiO$_2$−NH$_2$ nanoparticles was determined by using an XTT assay (Cell Signaling Technology, Danvers, MA). The XTT assay is based on the reduction of a colorless tetrazolium salt to a colored formazan product due to the activity of mitochondrial dehydrogenases in the mitochondria of living cells. The HT-29 cells were initially plated for 24 h in 96-well tissue culture
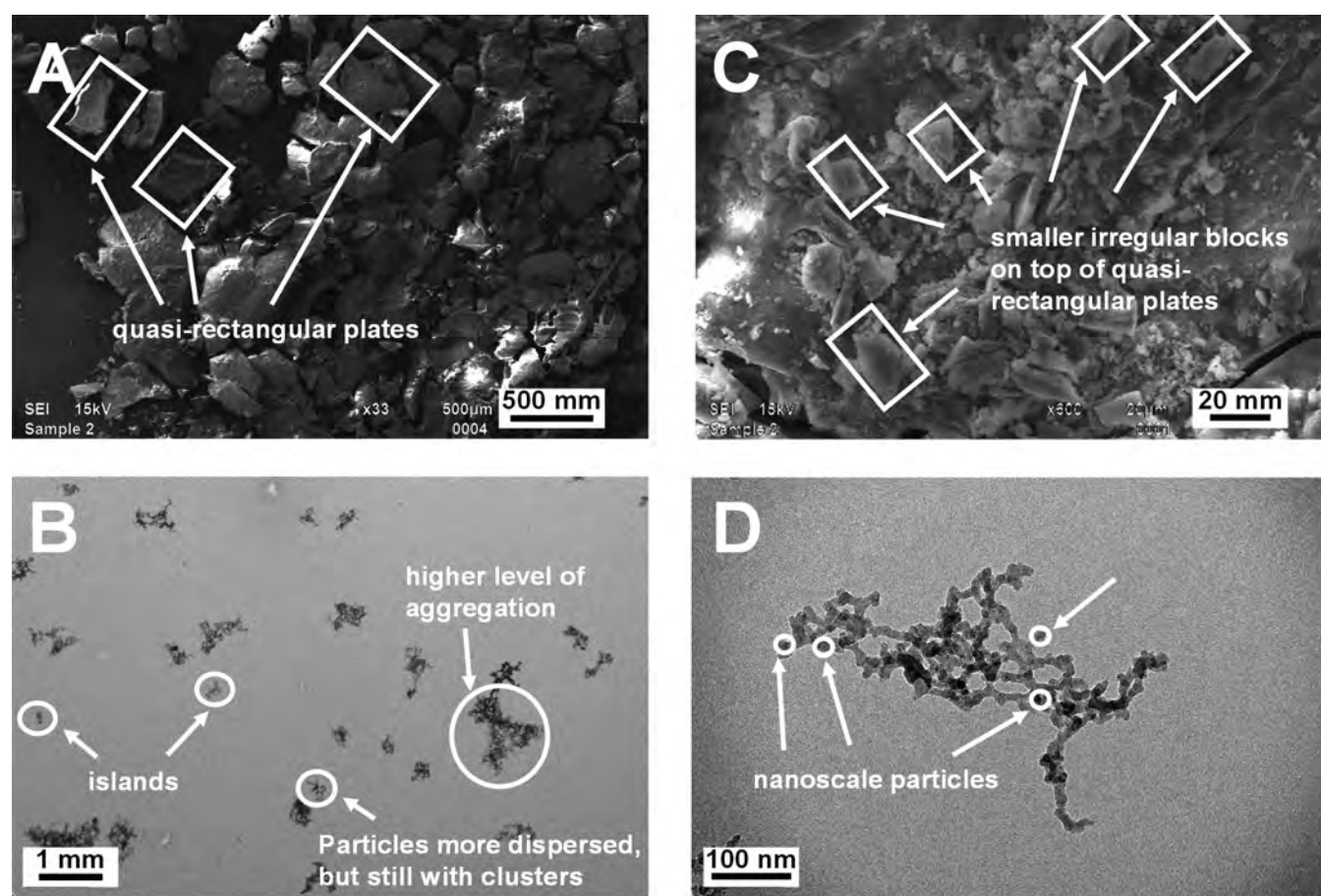
plates at a density of 5×10^3 per well. After 24 h, the cells were treated with 10, 100, and 1000 μg/mL of the EuDPA/SiO$_2$−NH$_2$ nanoparticle preparation for an additional 24 h. As a positive control for cytotoxicity, cells were treated with doxorubicin at 1.34 μM, a concentration representing ~2× the reported IC$_{50}$ in HT-29 cells.[28] As a negative control, cells were treated with vehicle (PBS) alone. The cells were treated at each concentration by using eight replicate wells for 24, 48, and 96 h. At each time point, the plates were subjected to the following treatment: 50 μL of XTT detection solution (a 1:50 ratio of electron coupling solution to XTT reagent) was added to each well containing 200 μL of medium. After 2 h incubation at 37 °C, the optical density (OD) of each well at 595 nm was measured by using a SpectraMax 190 plate reader (Molecular Devices, San Jose, CA).

2.10. Uptake of ^{177}Lu−EuDPA/SiO$_2$−NH$_2$ Nanoparticles. The time course of uptake of ^{177}Lu−EuDPA/SiO$_2$−NH$_2$ nanoparticles into HT-29 cells was determined by gamma scintillation counting using a model CRC-55tx dose calibrator/well counter (Capintec, Florham Park, NJ). The HT-29 cells were initially plated for 24 h in 35 mm dishes at a density of 1.5×10^5 per well in DMEM medium supplemented with 10% fetal bovine serum, 50 U/mL penicillin, and 50 mg/mL streptomycin. After 24 h, the medium was removed, and the cells were treated by the addition of 4081 MBq (110.3 mCi) ^{177}Lu−EuDPA/SiO$_2$−NH$_2$ in 1.0 mL of medium. At each time point after the addition, the cells were harvested by trypsinization, washed twice with PBS, and counted. The uptake of increasing doses of ^{177}Lu−EuDPA/SiO$_2$−NH$_2$ nanoparticles into HT-29 cells was also determined by gamma scintillation counting. The HT-29 cells were initially plated for 24 h in 35 mm dishes at a density of 1.5×10^5 per well in DMEM medium. After 24 h, the medium was removed, and the cells were treated with increasing amounts of ^{177}Lu−EuDPA/SiO$_2$−NH$_2$ nanoparticles at 6.52, 13.93, 30, 57.7, 113.2, and 224 mCi in 1.0 mL of medium. At 24 h after the addition, the cells were harvested by trypsinization and washed twice with PBS, and the cell pellets were counted. The uptake percentage was calculated as the amount of radioactivity associated with the cell pellet divided by the total radioactivity of the cell sample and medium.

2.11. SPECT Imaging. HT-29 tumors were established by subcutaneous injection of 0.2 mL into the right flanks of six mice at a concentration of 0.5×10^8 cells/mL resuspended in a 1:1 mixture of PBS and Matrigel extracellular matrix preparation (Corning, Oneonta, NY). On day 17, after initial HT-29 injection, the mice were injected intratumorally with 37 MBq (1.0 mCi) of ^{177}Lu−EuDPA/SiO$_2$−NH$_2$ nanoparticles in 100 μL of PBS, and image acquisition was started at 60 min afterward. Similarly, three mice were injected with ~37 MBq (1.0 mCi) of ^{177}LuCl$_3$ in 100 μL of PBS. The animals were anesthetized with isoflurane and fixed in a prone position on the bed and center of rotation relative to the gantry of a dedicated small animal SPECT/CT system (TriFoil Imaging, Northridge, CA). After 60 min, 3D SPECT imaging was performed in a step-and-shoot manner using the following acquisition parameters: 64 projections, 30 s/projection (35 min image acquisition), with a 208 keV photopeak ±10% window. SPECT 3D reconstruction was performed by using Avizo 9.0.1 software (Thermo Fisher Scientific, Waltham, MA). Immediately after SPECT imaging was performed, CT images were acquired by using the same coordinates as SPECT with 256 projections and 1024×1024 projection matrix size and a voltage of 60 kV; reconstructions were performed by using filtered back-projections.

2.12. HT-29 Xenograft Mouse Model. Female 3−6 week old athymic nude mice (Envigo RMS, Indianapolis, IN) were used for all in vivo studies. All animal experiments were performed in compliance with the Institutional Animal Care and Use Committee (IACUC) guidelines of Louisiana State University, through which humane care of animals was ensured. A colorectal tumor xenograft model was established by subcutaneous injection of 0.2 mL of HT-29 cells into the right flanks of 15 mice at a concentration of 5×10^7 cells/mL resuspended in a 1:1 mixture of PBS and Matrigel extracellular matrix preparation (Corning, Oneonta, NY). On day 5, after initial HT-29 injection, the mice were randomized into three groups of five mice,

Figure 2. Representative images obtained by scanning electron microscopy (A, B) and transmission electron microscopy (C, D) of EuDPA/SiO$_2$–NH$_2$ nanoparticles.

and the tumor dimensions of each mouse were measured with digital calipers. Tumor volumes were calculated employing eq 3

$$V = D \times d^2 \times 0.52 \tag{3}$$

where V is the tumor volume, D is the largest tumor dimension, and d is the smallest tumor dimension. After 17 days, the tumors reached an injectable size and were treated by a single intratumoral administration of 37 MBq (1.0 mCi) ^{177}Lu–EuDPA/SiO$_2$–NH$_2$ nanoparticles in 100 μL of PBS (group 1) or 37 MBq (1.0 mCi) ^{177}LuCl$_3$ in 100 μL of PBS (group 2). Control mice (group 3) received 100 μL of PBS alone. On day 34, after the initial HT-29 injection, the mice were humanely euthanized.
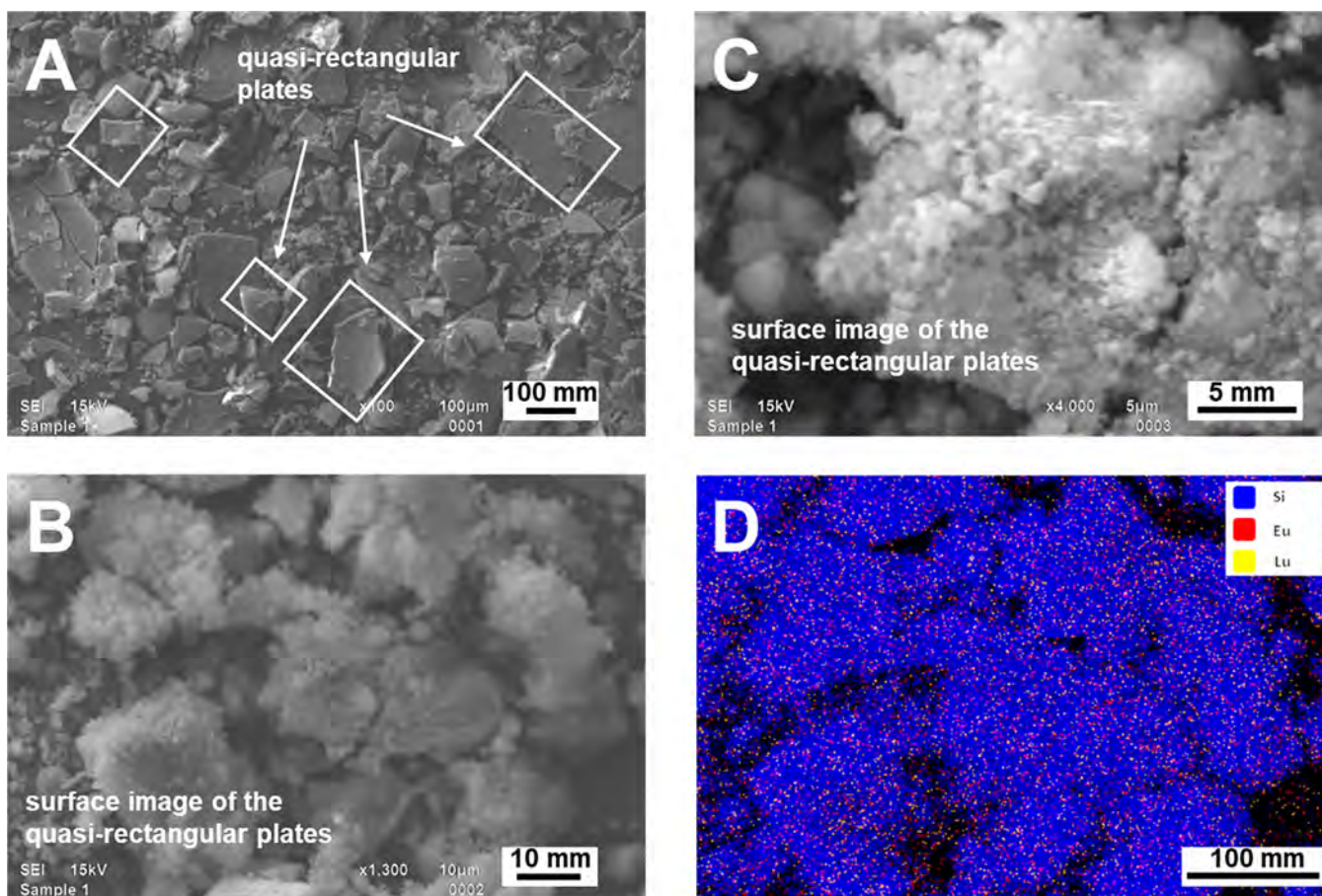
2.13. Biodistribution of ^{177}Lu–EuDPA/SiO$_2$–NH$_2$ Hybrid Nanoparticles after *In Vivo* Injection. The HT-29 tumor model was established by subcutaneous injection of 0.2 mL into the right flanks of six mice at a concentration of 0.5 × 10^8 cells/mL resuspended in a 1:1 mixture of PBS and Matrigel extracellular matrix preparation (Corning, Oneonta, NY). On day 17, after the initial HT-29 injection, the mice were randomized into two groups of three mice each. One group of mice was treated by an intratumoral administration of 37 MBq (1.0 mCi) ^{177}Lu–EuDPA/SiO$_2$–NH$_2$ nanoparticles in 100 μL of PBS, and a second group was treated by an intratumoral administration of 37 MBq (1.0 mCi) ^{177}LuCl$_3$ in 100 μL of PBS. At 48 h after treatment, the mice were humanely euthanized, and organs and blood were collected for determination of weights. Radioactivity associated with the organs and tissues was determined by using a model CRC-55tx dose calibrator/well counter (Capintec, Florham Park, NJ).

3. RESULTS AND DISCUSSION

3.1. Morphology and Chemical Evaluation. TEM and SEM images were acquired to characterize the synthesis of the EuDPA/SiO$_2$–NH$_2$ nanoparticles and elucidate the morphological properties of the product. SEM images obtained at different magnifications (Figures 2A and 2C) revealed the formation of small blocks with irregular morphology. The results of TEM (Figures 2B and 2D) showed that the EuDPA/SiO$_2$–NH$_2$ product was formed by small particles with sizes of <20 nm. It is important to emphasize that the particles had a morphology similar to those published in the literature.[29−31] These results confirmed the material composition as a nanocarrier and strengthened the use of the system proposed in this work.

Particle size analysis was also performed by using the DLS technique for the silica nanoparticles (without EuDPA) and the EuDPA/SiO$_2$–NH$_2$ compound, as shown in Figures S1A and S1B, respectively. This analysis revealed that the silica particles had an average particle size of 21.7 nm, while the EuDPA/SiO$_2$–NH$_2$ particles had an average particle size equal to 63.3 nm. These results indicate that the EuDPA/SiO$_2$–NH$_2$ compound was maintained at the nanoscale, and the insertion of the EuDPA complex into the nanoparticle structure favored an increase in particle size.

A Lu$_{0.5}$–Eu$_{0.5}$DPA/SiO$_2$–NH$_2$ nanoparticle formulation was synthesized and characterized by transmission electron microscopy (Figures 3A−C) to determine whether there was a perturbation of nanoparticles by the occupation of lutetium
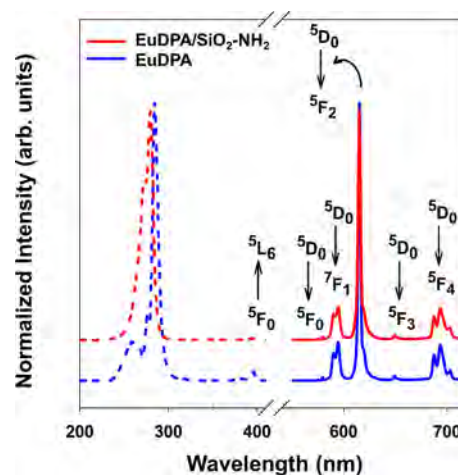
Figure 3. Representative images obtained by scanning electron microscopy (A−C) and EDS mapping analysis (D) of $Lu_{0.5}-Eu_{0.5}DPA/SiO_2-NH_2$ nanoparticles.

Table 1. Elemental Quantitative Analysis with the Atomic and Mass Percentages Obtained by EDS for the Compound $Lu_{0.5}-Eu_{0.5}DPA/SiO_2-NH_2$

element (%)	mass (%)	atomic (%)	std error (%)
C	32.8	45.5	9.9
O	38.9	40.5	8.7
Si	22.0	13.2	3.2
Eu	3.0	0.4	21.3
Lu	3.3	0.4	36.6

in preparation of the $^{177}Lu-EuDPA/SiO_2-NH_2$ radiopharmaceutical. We observed that the compound presented a morphology similar to $EuDPA/SiO_2-NH_2$, with the presence of small irregular blocks indicating that the introduction of the lutetium ion in the material did not affect the morphology of the nanomaterial.

Mapping of the $Lu_{0.5}-Eu_{0.5}DPA/SiO_2-NH_2$ compound using EDS spectroscopy was also performed (Figure 3D). These results showed that the nanomaterial consists of a higher amount of Si (13%) among the inorganic elements present. In addition, we observed that the atomic percentages of europium and lutetium found within the material were the same (0.4%), indicating that there was no preference in the introduction of the metallic ions in the silicon matrix and that the lanthanides were distributed throughout the uniformly. The identification of all elements is most evident from the analysis of the EDS spectrum shown in Figure S2. The quantitative representation

Figure 4. Excitation (dotted line) and emission (full line) spectra for EuDPA (λ_{Ex} = 283 nm; λ_{Em} = 615 nm; blue line) and $EuDPA/SiO_2-NH_2$ (λ_{Ex} = 279 nm; λ_{Em} = 615 nm; red line) compounds obtained at room temperature. EuDPA was obtained in aqueous solution at 1×10^{-5} mol/L and $EuDPA/SiO_2-NH_2$ in the form of a suspension of particles in PBS (pH = 7.4; 100 μg/mL).

of mass percentages and atomic percentage for the elements present in the sample is shown in Table 1.

3.2. Chemical, Thermal, and Compositional Analyses. For the characterization of the $EuDPA/SiO_2-NH_2$ compound, it was necessary to know in greater detail the main functional
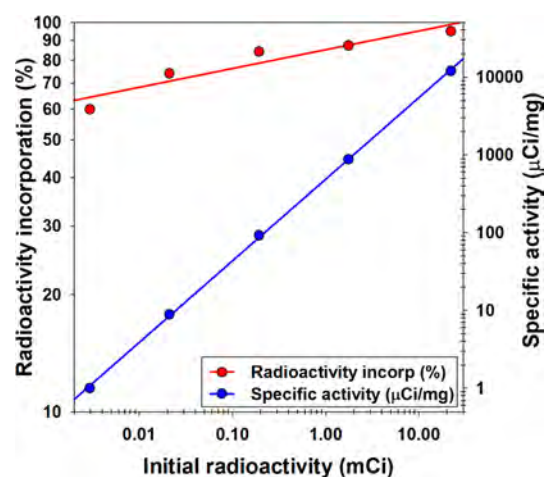
Table 2. Experimental Values for Radioactive (A_{rad}) and Nonradioactive (A_{nrad}) Decays, Lifetime (τ), and Quantum Efficiency (η) for EuDPA and EuDPA/SiO$_2$−NH$_2$

compound	A_{rad} (s^{-1})	A_{nrad} (s^{-1})	τ (ms)	η (%)
EuDPA	322.6	1805.0	0.47	15
EuDPA/SiO$_2$−NH$_2$	228.0	2297.8	0.31	7

groups present in the dipicolinic acid (H$_2$DPA); for this reason, the nanoparticles were subjected to FT-IR spectroscopy (Figure S3). The spectrum of the H$_2$DPA (black line) showed a broad and medium intensity band in the region of 3300−2500 cm^{-1} due to the O−H stretching of the carboxylic acid located at the ligand.[32] It was also possible to identify the carbonyl signal (C=O) by a single band of narrow and very pronounced profile located at 1701 cm^{-1}.[32] Also, for the carbonyl signal, the C-O-H out-of-plane bending was represented by a median intensity signal centered at 1419 cm^{-1} as well as a signal at 939 cm^{-1} that was a correlated plane with the intermolecular hydrogen bonds present in the solid. The symmetrical C−O stretch with a signal located at 1254 cm^{-1} [32] was also verified. The presence of the aromatic ring was present as evidenced by the observation of the C=C stretches of the ring, composed of three signals at 1569, 1538, and 1462 cm^{-1}, as well as those of the asymmetric and symmetric C−H stretches at 2962 and 2871 cm^{-1}, respectively.[32,33]
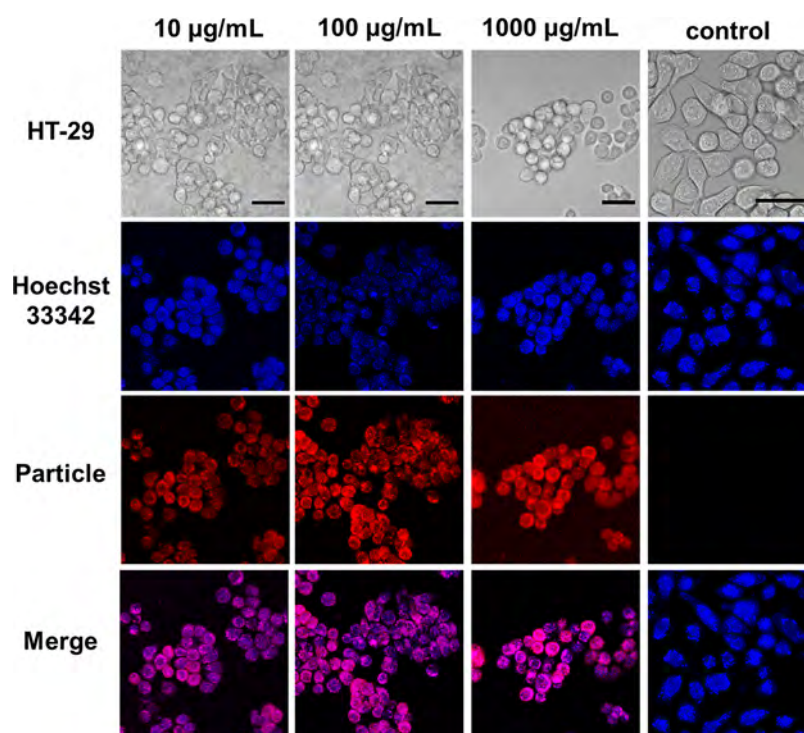
After the identification of the main functional groups of the H$_2$DPA, it was possible to perform a comparative analysis of the EuDPA metal complex with greater confidence (Figure S3, blue line). Initially, the asymmetric ν_{ASS}(COO$^-$) stretch of the carbonyl (1591 cm^{-1}) was displaced with respect to the C=O
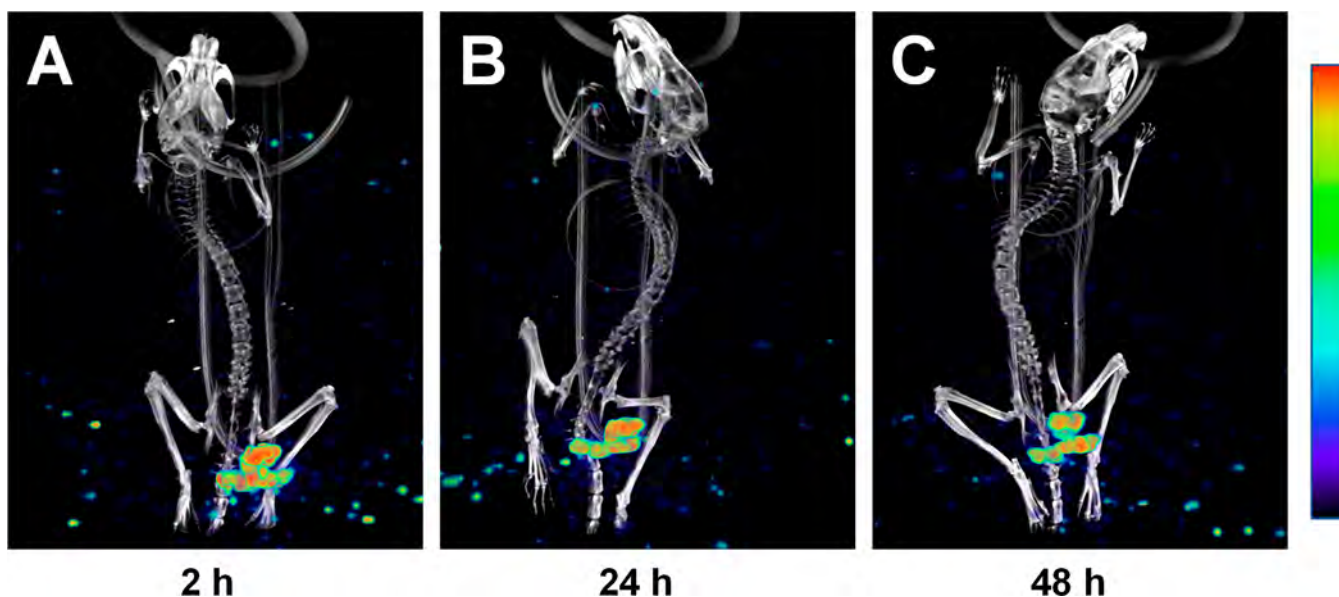

Figure 6. Measurement of nanoparticles as determined by % radioactivity incorporation or specific activity as a function of the initial input radioactivity for the synthesis of ^{177}Lu−EuDPA/SiO$_2$−NH$_2$.

signal from the ligand (1701 cm^{-1}), and this was due to deprotonation of carbonyl and coordination of this group with the metal ion, which provides a reduction of the frequency of molecular vibration and appearance of its band at a wavenumber lower than that observed for the free ligand.[30,31]
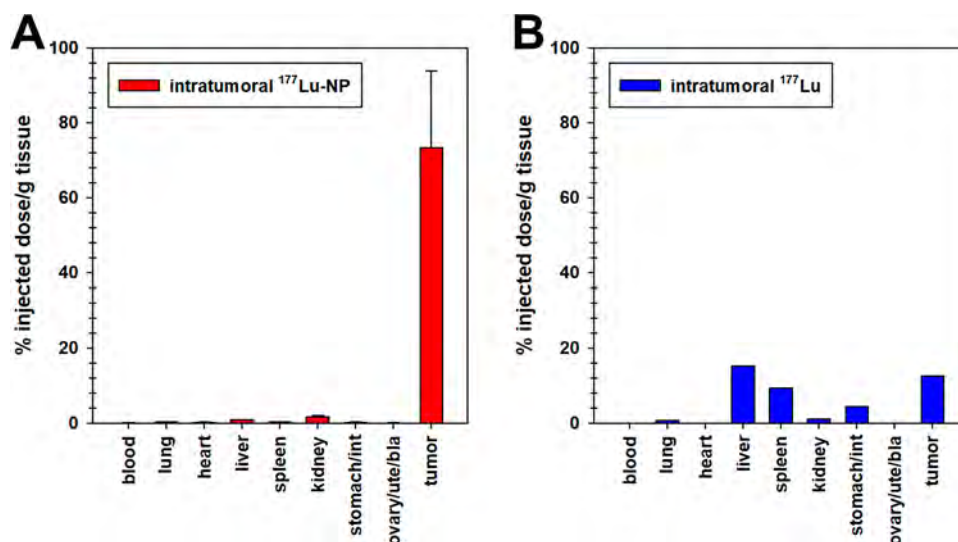
Analysis of the EuDPA/SiO$_2$−NH$_2$ nanoparticles was also performed by using the FT-IR spectroscopy technique, as shown in Figure S3 (red line). This analysis revealed the presence of a broad and intense band with maximum centering at 1070 cm^{-1}, which is related to the asymmetric stretching Si−O−Si from silane-derived groups. The functionalization

Figure 5. Representative confocal fluorescence microscopy images (63× magnification) of HT-29 cells treated with EuDPA/SiO$_2$−NH$_2$ (λ_{Ex} = 279 nm; λ_{Em} = 500−700 nm), as shown in red (Particle) obtained at concentrations of 10, 100, and 1000 μg/mL in PBS (pH 7.4). The cells were counterstained with Hoechst 33342 (λ_{Ex} = 350 nm; λ_{Em} = 461 nm), as shown in blue. Colocalization is shown as magenta in the merged images. Scale bars are 50 μm.

Figure 7. Coronal views of three-dimensional images after fusion of SPECT maximum intensity projection (MIP) and CT volume rendering images obtained at (A) 2, (B) 24, and (C) 48 h after injection of $^{177}Lu-EuDPA/SiO_2-NH_2$ nanoparticles intratumorally into athymic nude mice bearing HT-29 subcutaneous tumors.
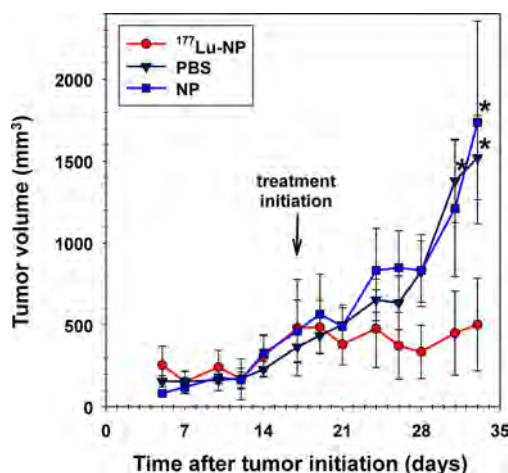

Figure 8. Evaluation of biodistribution of (A) $^{177}Lu-EuDPA/SiO_2-NH_2$ (^{177}Lu-NP) nanoparticles and (B) $^{177}LuCl_3$ (^{177}Lu) following intratumoral administration in athymic nude mice. Each bar represents the mean ± SEM measurements of three mice.

with $-NH_2$ groups could be identified by the presence of a weak band localized at 800 cm^{-1} due to the N−H vibrations directed outside the plane.[30,31] In addition, a signal in the centered at 1562 cm^{-1}, referring to the angular deformation N−H for primary amine, was observed. The EuDPA/SiO$_2$−NH$_2$ compound also exhibited a low-intensity, maximum centered signal at 1637 cm^{-1}, which was attributed to the asymmetric $\nu_{ASS}(COO^-)$ stretch of the coordination complex incorporated into SiO$_2$ nanoparticles.[30,31] These results suggested that the complex was internalized in the rigid silicon network in its original conformation, which stabilized the hybrid system by supramolecular interactions.

TGA analysis was also a necessary experimental approach both to support the characterization of the EuDPA metal complex and to determine the thermal stability profile of the EuDPA and EuDPA/SiO$_2$−NH$_2$ compounds. Concerning the

thermal behavior of EuDPA, we observed its decomposition into two fractions (Figure S4A). In the first thermal event, we observed the elimination of 14% mass in the temperature range between 30 and 150 °C occurring in two stages, which was attributed to the removal of seven molecules of water, hydration, and coordination, present in the coordination complex. The second heat event was related to the organic part of the DPA^{2-} coordinate ligand that was eliminated in three steps, totaling 45% of mass loss in the temperature range between 150 and 800 °C, giving the compound two ligands coordinated to the ion metallic. Thus, the chemical composition of the synthesized complex revealed good agreement with the theoretically proposed structure Eu-(DPA)$_2$(3H$_2$O)]·4H$_2$O,[20] as shown in Table S1.

TGA analysis for the EuDPA/SiO$_2$−NH$_2$ nanoparticles was performed between the 25 and 600 °C regions, as shown in

Figure 9. Evaluation of the therapeutic potential of the ^{177}Lu−EuDPA/SiO$_2$−NH$_2$ nanoparticles (^{177}Lu-NP) by measuring tumor volume as a function of time after intratumoral administration, compared to treatment with EuDPA/SiO$_2$−NH$_2$ nanoparticles (NP) or with a negative control (PBS). Each bar represents the mean ± SEM measurements of five mice. *$P < 0.05$ compared to ^{177}Lu-NP.

Figure S4B. We observed that the compound showed two mass events up to the production of waste from the elimination of 25% of the starting mass of the compound. It is important to note that the thermogram found for EuDPA/SiO$_2$−NH$_2$ resembles that described in the literature for SiO$_2$ nanoparticles.[34] In addition, these results were found to agree with reported data, in which compounds derived from SiO$_2$ nanoparticles have the percentage of remaining mass increased with the addition of the other components.

3.3. Spectroscopic Properties. The optical behavior of the EuDPA and EuDPA/SiO$_2$−NH$_2$ compounds was analyzed by using excitation, emission spectra, and lifetime analysis. The excitation spectrum for the EuDPA complex, obtained by monitoring λ_{Em} = 615 nm (Figure 4; dotted blue line), presented two bands in the region between 240 and 310 nm, with a maximum centered at 283 nm referring to the $\pi \rightarrow \pi^*$ transition of the DPA^{2-} ligand. It was also possible to observe the presence of a lower intensity signal centered at 395 nm, which was related to the $^5F_0 \rightarrow {}^5L_6$ transition of the Eu^{3+} ion. The emission spectrum for EuDPA, using λ_{Ex} = 283 nm (Figure 3, solid blue line), revealed the transitions $^5D_0 \rightarrow {}^7F_J$ (where J = 0, 1, 2, 3, and 4) typically related to the 4f^6 configuration of the Eu^{3+} ion. Additional analysis of the emission spectrum also demonstrated the absence of emission bands from the ligand, indicating that the ligand−metal energy conversion happened efficiently (i.e., antenna effect). In addition, the spectrum revealed the presence of the $^5D_0 \rightarrow {}^7F_0$ transition, which indicates the constraint of the point symmetry surrounding the ion for the representations C_n, C_{nv}, and C_s. It is important to note that the emission profile for the EuDPA compound was analogous to that reported previously in the literature.[20]

The photoluminescence analysis for the EuDPA/SiO$_2$−NH$_2$ compound was also evaluated by its excitation spectra (Figure 4, dotted red line) and emission (Figure 4, solid red line). The excitation spectrum, obtained by monitoring λ_{Em} = 615 nm, revealed the presence of two bands in the region between 240 and 310 nm, with a maximum centered at 279 nm referring to the $\pi \rightarrow \pi^*$ transition of the DPA^{2-} ligand, although with a slightly different profile from the observed for the EuDPA

(Figure 3; dotted blue line). This difference is likely related to the organization of the EuDPA complex, which was immobilized in the solid state in the form of EuDPA/SiO$_2$−NH$_2$ nanoparticles. The emission spectrum for the EuDPA/SiO$_2$−NH$_2$ had the same spectral profile as that presented for the EuDPA (Figure 4; solid blue line), indicating that the complex incorporated in the hybrid network conferred the same point symmetry around the ion in relation to the free coordination complex. The comparison between the excitation (λ_{Em} = 615 nm) and emission (λ_{Ex} = 283 nm) spectra between the EuDPA/SiO$_2$−NH$_2$ (blue lines) and Lu$_{0.5}$−Eu$_{0.5}$DPA/SiO$_2$−NH$_2$ (red lines) was also performed, as shown in Figure S5. We observed that the excitation and emission spectral patterns did not change, indicating that the introduction of lutetium did not cause changes in the chemical environment of the EuDPA complex within the hybrid compound.

The exponential decays for the $^5D_0$ emitter state were determined from the exponential decay curve of the EuDPA and EuDPA/SiO$_2$−NH$_2$ compounds (Figures S6A and S6B). The curves of both materials presented a monoexponential profile, indicating the existence of only one emitter metal site for each system. It was also observed that the EuDPA compound (Figure S6B) showed a low quantum emission efficiency in relation to the usual complexes of europium,[35] equal to 18%, that is associated with a high nonradiative decay (A_{nrad} = 340.5 s^{-1}). In addition, the compound had a low lifetime rate (τ = 0.47 ms) that contributed to a quantum emission efficiency. This photoluminescent parameter can be explained by the presence of energy states from the O−H oscillators of the water, which is resonant to the $^5D_0$ emitter state of Eu^{3+}, promoting the deactivation of the luminescence. Consequently, this effect resulted in a low quantum emission efficiency when compared to similar results in the literature by using other solvents.[20,36]

The analysis of exponential decay curves for the EuDPA/SiO$_2$−NH$_2$ also presented a low value for the radiative decay rate (A_{rad} = 228.0 s^{-1}), while the value for the nonradiative decay was high (A_{nrad} = 2297.8 s^{-1}). This fact, combined with a reduction in lifetime (τ = 0.31 ms), when applying the radiative decay curve of Figure S6B, indicated a recovery of quantum efficiency of emission equal to 7%. The experimental values for the radiative (A_{rad}) and nonradiative (A_{nrad}) decays and quantum emission (η) for EuDPA and EuDPA/SiO$_2$−NH$_2$ are presented in Table 2.

3.4. Fluorescence Microscopy Imaging of the HT-29 Cell Line. The EuDPA/SiO$_2$−NH$_2$ nanoparticles were analyzed for cellular uptake by using confocal microscopy experiments. In this approach, the particle internalization was examined in HT-29 cells at concentrations 10, 100, and 1000 μg/mL after a 24 h incubation period.

As shown in Figure 5, we observed that the nanoparticles showed good uptake into HT-29 cells in vitro, with no indication of any morphological changes. Strong cytoplasmic fluorescence could be observed, represented by the accumulation of luminescent particles. This evidence of uptake suggested that the EuDPA/SiO$_2$−NH$_2$ nanoparticles are promising in the composition of luminescent biomarkers. In addition, the cytotoxicity of EuDPA/SiO$_2$−NH$_2$ was tested on HT-29 cells by using an XTT assay to assess the biocompatibility of the nanoparticles. The assays performed revealed that cellular viability was not significantly affected by the nanoparticles at the concentrations tested (Figure S7) after treatment for 24 or 48 h.

3.5. Radioincoporation of ^{177}Lu into the Luminescent Nanoparticle. The EuDPA/SiO$_2$−NH$_2$ nanoparticle was next used as a carrier for incorporating the ^{177}Lu radioisotope as a constituent (^{177}Lu−EuDPA/SiO$_2$−NH$_2$). The strategy employed was based on the incorporation via the one-pot radioisotope method in the formation of a hybrid silica nanoparticle material. To quantify the incorporation percentage of ^{177}Lu, we determined the ratio of the amount of radioactivity between the compound before and after the ^{177}Lu−EuDPA/SiO$_2$−NH$_2$ synthesis.

For this assessment, the amount of radioisotope added to the reaction was varied to obtain the best radioincorporation conditions. The introduction of higher initial amounts of ^{177}LuCl$_3$ ranging from 0.109 to 814 MBq (2.94 to 22 mCi) into the reaction mixture resulted in increasing incorporation into ^{177}Lu−EuDPA/SiO$_2$−NH$_2$ nanoparticles ranging from 60% to 93% (Figure 6). Based on the incorporation of ^{177}Lu into the EuDPA/SiO$_2$-NH$_2$ nanoparticles, the values for the specific activities of the material (defined as the ratio of radioactivity to the unit mass) were determined. Using a calculation of the synthesis of EuDPA/SiO$_2$−NH$_2$ particles that generated a mass equal to 1.75 ± 0.50 mg, we found that the log values of specific activities for the compound showed a linear relationship to the amount of initial (input) radioactivity (Figure 6).

3.6. Cellular Uptake of ^{177}Lu−EuDPA/SiO$_2$−NH$_2$. The uptake of radiolabeled nanoparticles by HT-29 cells was measured by the amount of radioactivity incorporated after treatment with the ^{177}Lu-radiolabeled nanoparticles. As shown in Figure S8A, the relationship between the incubation time and the uptake of the ^{177}Lu−EuDPA/SiO$_2$−NH$_2$ nanoparticles was determined. We observed that there was a rapid increase in the incorporation of radioactivity that was maximal at 28.1% after 1 h. This accumulation was followed by a slower loss of radioactivity over time to 10.8% after 24 h of incubation. A dose response curve associated with the uptake at 24 h of the ^{177}Lu−EuDPA/SiO$_2$−NH$_2$ nanoparticles was also determined (Figure S8B). As the concentration of ^{177}Lu−EuDPA/SiO$_2$−NH$_2$ increased, there was a concomitant increase in % binding and uptake as measured by radioactivity associate with the HT-29 cells that demonstrated a maximum uptake at ∼16%.

3.7. *In Vivo* SPECT Imaging Experiments. In a preclinical study to understand the biodistribution of the radiolabeled nanoparticles, SPECT/CT imaging was used for *in vivo* detection. In this experiment, 74 MBq (2.0 mCi) ^{177}Lu−EuDPA/SiO$_2$−NH$_2$ was injected intratumorally into athymic nude mice bearing subcutaneous HT-29 tumors. Subsequently, SPECT/CT images were acquired at (A) 2 h, (B) 24 h, and (C) 48 h after administration. As shown in Figure 7, visible accumulation was detected at 2 h in the subcutaneous HT-29 tumor on the left flank of a nude mouse, which remained present with a similar SPECT signal pattern for the or localization at 24 and 28 h after injection of ^{177}Lu−EuDPA/SiO$_2$−NH$_2$. These results suggest that, once injected, there is little subsequent diffusion away from the tumor site. As a control, free ^{177}LuCl$_3$ injected intravenously into a mouse did not accumulate in the tumor, and there was no visible signal by SPECT/CT imaging (data not shown).

Immediately following the SPECT/CT imaging at 48 h, the animals were euthanized, and selected organs were dissected for further analyses. The radioactivity of the tissue samples was measured by using a well counter and expressed as % injected dose/g tissue weight. The *in vivo* biodistribution results of the dissection analysis are summarized in Figure 8. Similar to the results observed in the SPECT images, most of the radioactivity in mice treated with ^{177}Lu−EuDPA/SiO$_2$−NH$_2$ was found in the tumor (>70%), with limited radioactivity in the other organs measured (Figure 7A). In contrast, a control mouse injected with free ^{177}LuCl$_3$ intratumorally showed radioactivity in the liver, spleen, and stomach/intestine as well and kidney and lung. These results support the retention of radioactivity at the tumor site by using ^{177}Lu−EuDPA/SiO$_2$−NH$_2$ nanoparticles and their potential use as an imaging agent.

3.8. Evaluation of Therapeutic Potential. A subcutaneous mouse model of colorectal cancer was used to investigate the therapeutic potential of the ^{177}Lu−EuDPA/SiO$_2$−NH$_2$ nanoparticles. For this approach, athymic nude mice were injected subcutaneously with 1×10^7 HT-29 cells. At 16 days after the initial injection, when the tumors reached ∼500 mm^3, the mice in one group (*n* = 5) were treated with a single intratumoral injection of ^{177}Lu−EuDPA/SiO$_2$−NH$_2$. The second group of mice (*n* = 5) was treated with a single intratumoral injection of EuDPA/SiO$_2$−NH$_2$ as a negative control; the third group (*n* = 5) was treated with a single intratumoral injection of PBS as a no treatment control.

As shown in Figure 9, the treatment of mice with ^{177}Lu−EuDPA/SiO$_2$−NH$_2$ resulted in significant inhibition of tumor growth. In comparison, the treatment of mice with a nonradioactive control EuDPA/SiO$_2$−NH$_2$ did not affect tumor growth compared to mice receiving PBS treatment alone. Tumor growth in these groups continues exponentially until the experiment was terminated on day 33. Biodistribution and dosimetry studies of therapeutic biomolecules radiolabeled with ^{177}Lu have been performed.[37,38] Based on these findings, future *in vivo* studies will need to be performed to assess the biosafety and determine the radiation-absorbed doses from ^{177}Lu−EuDPA/SiO$_2$−NH$_2$ administration.

As a proof of principle for preclinical application, we performed a direct intratumoral injection of ^{177}Lu−EuDPA/SiO$_2$−NH$_2$ nanoparticles. This locoregional approach could potentially be used as an alternative to the systemic administration of drugs for the treatment of localized tumors. However, in the case of metastatic disease, intratumoral nanoparticle delivery would not be feasible. Instead, a targeted distribution would be necessary to reach distant sites. One approach to the delivery of nanoparticles to a tumor site has consisted of passive targeting, mainly through the enhanced permeability and retention (EPR) effect after systemic administration.[39] Despite clinical efforts to exploit passive targeting approaches for drug delivery to cancer cells, only limited success has been achieved, likely due to nonselective targeting efficiency. Therefore, future directions to improve ^{77}Lu−EuDPA/SiO$_2$−NH$_2$ nanoparticles will include active targeting strategies[40] mediated by incorporating biological ligands (i.e., proteins, polysaccharides, aptamers, peptides, small molecules, etc.) with a high affinity toward cancer cell surface receptors.

4. CONCLUSIONS

In this study, we synthesized the compounds EuDPA and EuDPA/SiO$_2$−NH$_2$ and characterized them by SEM, FT-IR, TGA, and luminescence, which determined their chemical, morphological, and optical properties. Radiolabeling of EuDPA/SiO$_2$−NH$_2$ with ^{177}Lu showed efficient incorporation

into the final compound for use in SPECT imaging and radiotherapy using an HT-29 colon cancer preclinical model. These results support the use of $^{177}Lu-EuDPA/SiO_2-NH_2$ particles for imaging tumors and demonstrate their therapeutic potential for treating colorectal tumors *in vivo*.

■ ASSOCIATED CONTENT

Ⓢ Supporting Information

The Supporting Information is available free of charge at https://pubs.acs.org/doi/10.1021/acsanm.0c01427.

Table S1: thermogravimetric analysis used as a compositional estimation of the EuDPA complex; Figure S1: DLS analysis for SiO_2 nanoparticles (without EuDPA) and $EuDPA/SiO_2-NH_2$ nanoparticles; Figure S2: EDS spectrum for the analysis of $Lu_{0.5}-Eu_{0.5}DPA/SiO_2-NH_2$ nanoparticles; Figure S3: infrared spectra for H_2DPA, EuDPA, and $EuDPA/SiO_2-NH_2$; Figure S4: TGA of EuDPA and $EuDPA/SiO_2-NH_2$; Figure S5: excitation and emission spectra for $EuDPA/SiO_2-NH_2$ and $Lu_{0.5}-Eu_{0.5}DPA/SiO_2-NH_2$; Figure S6: exponential decay curves for EuDPA and $EuDPA/SiO_2-NH_2$; Figure S7: viability of HT-29 cells after treatment with $EuDPA/SiO_2-NH_2$; Figure S8: percent uptake of $^{177}Lu-EuDPA/SiO_2-NH_2$ into HT-29 cells (PDF)

■ AUTHOR INFORMATION

Corresponding Authors

Severino A. Junior − *Department of Fundamental Chemistry, Federal University of Pernambuco, Recife, Pernambuco 50670-901, Brazil;* Ⓞ orcid.org/0000-0002-8092-4224; Email: salvesjr@ufpe.br

J. Michael Mathis − *Department of Comparative Biomedical Sciences, School of Veterinary Medicine, Louisiana State University, Baton Rouge, Louisiana 70803, United States; Graduate School of Biomedical Sciences, University of North Texas Health Science Center, Fort Worth, Texas 76107, United States;* ⓄΟ orcid.org/0000-0001-5528-5195; Email: michael.mathis@unthsc.edu

Authors

Rodrigo da Silva Viana − *Department of Fundamental Chemistry, Federal University of Pernambuco, Recife, Pernambuco 50670-901, Brazil; Department of Chemistry and Department of Comparative Biomedical Sciences, School of Veterinary Medicine, Louisiana State University, Baton Rouge, Louisiana 70803, United States;* ⓄΟ orcid.org/0000-0003-1329-6958

Luciana Amaral de Mescana Costa − *Department of Animal Morphology and Physiology, Federal Rural University of Pernambuco, Recife, Pernambuco 52171-900, Brazil; Department of Comparative Biomedical Sciences, School of Veterinary Medicine, Louisiana State University, Baton Rouge, Louisiana 70803, United States;* ⓄΟ orcid.org/0000-0002-6899-2240

Ashlyn C. Harmon − *Department of Comparative Biomedical Sciences, School of Veterinary Medicine, Louisiana State University, Baton Rouge, Louisiana 70803, United States;* ⓄΟ orcid.org/0000-0001-8917-9745

Manoel Adrião Gomes Filho − *Department of Animal Morphology and Physiology, Federal Rural University of Pernambuco, Recife, Pernambuco 52171-900, Brazil;* ⓄΟ orcid.org/0000-0003-4458-8451

Eduardo H. L. Falcão − *Department of Fundamental Chemistry, Federal University of Pernambuco, Recife, Pernambuco 50670-901, Brazil;* ⓄΟ orcid.org/0000-0002-7408-6287

Maria G. H. Vicente − *Department of Chemistry, Louisiana State University, Baton Rouge, Louisiana 70803, United States;* ⓄΟ orcid.org/0000-0002-4429-7868

Complete contact information is available at:
https://pubs.acs.org/10.1021/acsanm.0c01427

■ ACKNOWLEDGMENTS

■ ABBREVIATIONS

APTES, 3-aminopropyltriethoxysilane; DMEM, Dulbecco's modified Eagle's medium; DLS, dynamic light scattering; EDS, energy dispersive X-ray spectrometry; FT-IR, Fourier transform infrared; IACUC, Institutional Animal Care and Use Committee; PBS, phosphate-buffered saline; DPA, pyrimidine-2,6-dicarboxylic acid; SEM, scanning electron microscopy; SPECT, single photon emission computerized tomography; TEOS, tetraethyl orthosilicate; TGA, thermogravimetric analysis; TEM, transmission electron microscopy; UV−vis, ultraviolet−visible; XTT, 2,3-bis(2-methoxy-4-nitro-5-sulfophenyl)-2H-tetrazolium-5-carboxanilide.

■ REFERENCES

(1) Keum, N.; Giovannucci, E. Global burden of colorectal cancer: Emerging trends, risk factors and prevention strategies. *Nat. Rev. Gastroenterol. Hepatol.* **2019**, *16* (12), 713−732.

(2) Häfner, M. F.; Debus, J. Radiotherapy for colorectal cancer: Current standards and future perspectives. *Visceral Medicine* **2016**, *32* (3), 172−7.

(3) Banerjee, S.; Pillai, M. R.; Knapp, F. F. Lutetium-177 therapeutic radiopharmaceuticals: linking chemistry, radiochemistry, and practical applications. *Chem. Rev.* **2015**, *115* (8), 2934−74.

(4) Dash, A.; Pillai, M. R.; Knapp, F. F. Production of ^{177}Lu for targeted radionuclide therapy: available options. *Nucl. Med. Mol. Imaging* **2015**, *49* (2), 85−107.

(5) Iravani, A.; Violet, J.; Azad, A.; Hofman, M. S. Lutetium-177 prostate-specific membrane antigen (PSMA) theranostics: Practical nuances and intricacies. *Prostate Cancer Prostatic Dis.* **2020**, *23* (1), 38−52.

(6) Ramos, A. P.; Cruz, M. A.; Tovani, C. B.; Ciancaglini, P. Biomedical applications of nanotechnology. *Biophys. Rev.* **2017**, *9* (2), 79−89.

(7) Enrique, M.-A.; Mariana, O.-R.; Mirshojaei, S. F.; Ahmadi, A. Multifunctional radiolabeled nanoparticles: strategies and novel

classification of radiopharmaceuticals for cancer treatment. *J. Drug Targeting.* **2015**, *23* (3), 191−201.

(8) McNamara, K.; Tofail, S. A. Nanoparticles in biomedical applications. *Adv. Physics: X.* **2017**, *2* (1), 54−88.

(9) Mirshojaei, S. F.; Ahmadi, A.; Morales-Avila, E.; Ortiz-Reynoso, M.; Reyes-Perez, H. Radiolabelled nanoparticles: novel classification of radiopharmaceuticals for molecular imaging of cancer. *J. Drug Targeting.* **2016**, *24* (2), 91−101.

(10) Wang, D.; Ren, Y.; Shao, Y.; Yu, D.; Meng, L. Facile preparation of doxorubicin-loaded and folic acid-conjugated carbon nanotubes@poly (N-vinyl pyrrole) for targeted synergistic chemo−photothermal cancer treatment. *Bioconjugate Chem.* **2017**, *28* (11), 2815−2822.

(11) Cheng, Y. J.; Qin, S. Y.; Ma, Y. H.; Chen, X. S.; Zhang, A. Q.; Zhang, X. Z. Super-pH-sensitive mesoporous silica nanoparticle-based drug delivery system for effective combination cancer therapy. *ACS Biomater. Sci. Eng.* **2019**, *5* (4), 1878−1886.

(12) Wang, J.; Zhang, Y.; Jin, N.; Mao, C.; Yang, M. Protein-induced gold nanoparticle assembly for improving the photothermal effect in cancer therapy. *ACS Appl. Mater. Interfaces* **2019**, *11* (12), 11136−11143.

(13) Choi, G. E.; Kang, M. S.; Kim, Y. J.; Yoon, J. J.; Jeong, Y. I. Magnetically responsive drug delivery using doxorubicin and iron oxide nanoparticle-incorporated lipocomplexes. *J. Nanosci. Nanotechnol.* **2019**, *19* (2), 675−679.

(14) Kulkarni, N. S.; Guererro, Y.; Gupta, N.; Muth, A.; Gupta, V. Exploring potential of quantum dots as dual modality for cancer therapy and diagnosis. *J. Drug Delivery Sci. Technol.* **2019**, *49*, 352−364.

(15) Zheng, Y.; You, X.; Guan, S.; Huang, J.; Wang, L.; Zhang, J.; Wu, J. Poly (ferulic acid) with an anticancer effect as a drug nanocarrier for enhanced colon cancer therapy. *Adv. Funct. Mater.* **2019**, *29* (15), 1808646.

(16) Ou, K.; Xu, X.; Guan, S.; Zhang, R.; Zhang, X.; Kang, Y.; Wu, J. Nanodrug Carrier Based on Poly (Ursolic Acid) with Self-Anticancer Activity against Colorectal Cancer. *Adv. Funct. Mater.* **2020**, *30* (9), 1907857.

(17) Kalhapure, R. S.; Renukuntla, J. Thermo-and pH dual responsive polymeric micelles and nanoparticles. *Chem.-Biol. Interact.* **2018**, *295*, 20−37.

(18) Sun, Q.; You, Q.; Wang, J.; Liu, L.; Wang, Y.; Song, Y.; Cheng, Y.; Wang, S.; Tan, F.; Li, N. Theranostic nanoplatform: triple-modal imaging-guided synergistic cancer therapy based on liposome-conjugated mesoporous silica nanoparticles. *ACS Appl. Mater. Interfaces* **2018**, *10* (2), 1963−1975.

(19) Carvalho, M. R.; Reis, R. L.; Oliveira, J. M. Dendrimer nanoparticles for colorectal cancer applications. *J. Mater. Chem. B* **2020**, *8* (6), 1128−1138.

(20) Wang, Y.; Zhao, Q.; Han, N.; Bai, L.; Li, J.; Liu, J.; Che, E.; Hu, L.; Zhang, Q.; Jiang, T.; Wang, S. Mesoporous silica nanoparticles in drug delivery and biomedical applications. *Nanomedicine* **2015**, *11* (2), 313−27.

(21) Watermann, A.; Brieger, J. Mesoporous silica nanoparticles as drug delivery vehicles in cancer. *Nanomaterials* **2017**, *7* (7), 189.

(22) Tao, C.; Du, K.; Yin, Q.; Zhu, J.; Yan, H.; Zhu, F.; Zhang, L. Pyridine-2, 6-dicarboxylic acid for the sensitization of Europium (III) luminescence with very long lifetimes. *RSC Adv.* **2015**, *5* (72), 58936−42.

(23) Stöber, W.; Fink, A.; Bohn, E. Controlled growth of monodisperse silica spheres in the micron size range. *J. Colloid Interface Sci.* **1968**, *26* (1), 62−9.

(24) Liu, M.; Ye, Y.; Yao, C.; Zhao, W.; Huang, X. Mn2+-doped NaYF4: Yb/Er upconversion nanoparticles with amplified electrogenerated chemiluminescence for tumor biomarker detection. *J. Mater. Chem. B* **2014**, *2* (38), 6626−33.

(25) Carnall, W. T.; Crosswhite, H.; Crosswhite, H. M. *Energy Level Structure and Transition Probabilities in the Spectra of the Trivalent Lanthanides in LaF₃*; Argonne National Lab.: Argonne, IL, 1978.

(26) de Mello Donegá, C.; Junior, S. A.; De Sa, G. F. Synthesis, luminescence and quantum yields of Eu (III) mixed complexes with 4,4,4-trifluoro-1-phenyl-1,3-butanedione and 1,10-phenanthroline-N-oxide. *J. Alloys Compd.* **1997**, *250* (1−2), 422−6.

(27) de Sá, G. F.; Malta, O. L.; de Mello Donegá, C.; Simas, A. M.; Longo, R. L.; Santa-Cruz, P. A.; da Silva, E. F. Spectroscopic properties and design of highly luminescent lanthanide coordination complexes. *Coord. Chem. Rev.* **2000**, *196* (1), 165−95.

(28) Nguyen, H. N.; Hoang, T. M.; Mai, T. T.; Nguyen, T. Q.; Do, H. D.; Pham, T. H.; Nguyen, T. L.; Ha, P. T. Enhanced cellular uptake and cytotoxicity of folate decorated doxorubicin loaded PLA-TPGS nanoparticles. *Adv. Nat. Sci.: Nanosci. Nanotechnol.* **2015**, *6* (2), 025005.

(29) Shah, K. W. Nanosynthesis techniques of silica-coated nanostructures, novel nanomaterials - synthesis and applications. *IntechOpen* **2018**, DOI: 10.5772/intechopen.74097.

(30) Shah, S. T.; Yehya, W. A.; Saad, O.; Simarani, K.; Chowdhury, Z.; Alhadi, A. A.; Al-Ani, L. A. Surface functionalization of iron oxide nanoparticles with gallic acid as potential antioxidant and antimicrobial agents. *Nanomaterials* **2017**, *7* (10), 306.

(31) Aygar, G.; Kaya, M.; Özkan, N.; Kocabıyık, S.; Volkan, M. Preparation of silica coated cobalt ferrite magnetic nanoparticles for the purification of histidine-tagged proteins. *J. Phys. Chem. Solids* **2015**, *87*, 64−71.

(32) Pavia, D. L.; Lampman, G. M.; Kriz, G. S.; Vyvyan, J. A. *Introduction to Spectroscopy*; Cengage Learning: 2008.

(33) Silverstein, R. M.; Webster, F. X.; Kiemle, D. J. *Spectrometric Identification of Organic Compounds*; John Wiley & Sons: Hoboken, NJ, 2005.

(34) Kim, Y. J.; Kim, J. H.; Ha, S. W.; Kwon, D.; Lee, J. K. Polyimide nanocomposites with functionalized SiO₂ nanoparticles: enhanced processability, thermal and mechanical properties. *RSC Adv.* **2014**, *4* (82), 43371−7.

(35) De Mello Donegá, C.; Junior, S. A.; De Sa, G. F. Europium (III) mixed complexes with *β*-diketones and o-phenanthroline-N-oxide as promising light-conversion molecular devices. *Chem. Commun.* **1996**, *10*, 1199−200.

(36) Stein, G.; Würzberg, E. Energy gap law in the solvent isotope effect on radiationless transitions of rare earth ions. *J. Chem. Phys.* **1975**, *62* (1), 208−13.

(37) Vilchis-Juárez, A.; Ferro-Flores, G.; Santos-Cuevas, C.; Morales-Avila, E.; Ocampo-García, B.; Díaz-Nieto, L.; Luna-Gutiérrez, M.; Jiménez-Mancilla, N.; Pedraza-López, M.; Gómez-Oliván, L. Molecular targeting radiotherapy with cyclo-RGDFK (C) peptides conjugated to 177Lu-labeled gold nanoparticles in tumor-bearing mice. *J. Biomed. Nanotechnol.* **2014**, *10* (3), 393−404.

(38) Nicolas, G. P.; Mansi, R.; McDougall, L.; Kaufmann, J.; Bouterfa, H.; Wild, D.; Fani, M. Biodistribution, pharmacokinetics, and dosimetry of 177Lu-, 90Y-, and 111In-labeled somatostatin receptor antagonist OPS201 in comparison to the agonist 177Lu-DOTATATE: the mass effect. *J. Nucl. Med.* **2017**, *58* (9), 1435−1441.

(39) Attia, M. F.; Anton, N.; Wallyn, J.; Omran, Z.; Vandamme, T. F. An overview of active and passive targeting strategies to improve the nanocarriers efficiency to tumour sites. *J. Pharm. Pharmacol.* **2019**, *71* (8), 1185−98.

(40) Yoo, J.; Park, C.; Yi, G.; Lee, D.; Koo, H. Active targeting strategies using biological ligands for nanoparticle drug delivery systems. *Cancers* **2019**, *11* (5), 640.